

**UCLA**

**UCLA Previously Published Works**

**Title**

Minimum conditions for the induction of cortical spreading depression in brain slices

**Permalink**

<https://escholarship.org/uc/item/5d221548>

**Journal**

Journal of Neurophysiology, 112(10)

**ISSN**

0022-3077

**Authors**

Tang, Yujie T  
Mendez, Jorge M  
Theriot, Jeremy J  
et al.

**Publication Date**

2014-11-15

**DOI**

10.1152/jn.00205.2014

Peer reviewed

# Minimum conditions for the induction of cortical spreading depression in brain slices

Yujie T. Tang, Jorge M. Mendez, Jeremy J. Theriot, Punam M. Sawant, Héctor E. López-Valdés, Y. Sungtaek Ju and K. C. Brennan

*J Neurophysiol* 112:2572-2579, 2014. First published 13 August 2014; doi:10.1152/jn.00205.2014

## You might find this additional info useful...

---

This article cites 54 articles, 14 of which can be accessed free at:

</content/112/10/2572.full.html#ref-list-1>

Updated information and services including high resolution figures, can be found at:

</content/112/10/2572.full.html>

Additional material and information about *Journal of Neurophysiology* can be found at:

<http://www.the-aps.org/publications/jn>

---

This information is current as of January 14, 2015.

## Minimum conditions for the induction of cortical spreading depression in brain slices

Yujie T. Tang,<sup>1</sup> Jorge M. Mendez,<sup>2</sup> Jeremy J. Theriot,<sup>2</sup> Punam M. Sawant,<sup>2</sup>  
Héctor E. López-Valdés,<sup>3</sup> Y. Sungtaek Ju,<sup>1\*</sup> and K. C. Brennan<sup>2\*</sup>

<sup>1</sup>Department of Mechanical and Aerospace Engineering and Department of Bioengineering, University of California, Los Angeles, California; <sup>2</sup>Department of Neurology, University of Utah, Salt Lake City, Utah; and <sup>3</sup>Department of Neurology, University of California, Los Angeles, California

Submitted 14 March 2014; accepted in final form 12 August 2014

**Tang YT, Mendez JM, Theriot JJ, Sawant PM, López-Valdés HE, Ju YS, Brennan KC.** Minimum conditions for the induction of cortical spreading depression in brain slices. *J Neurophysiol* 112: 2572–2579, 2014. First published August 13, 2014; doi:10.1152/jn.00205.2014.—Cortical spreading depression (CSD) occurs during various forms of brain injury such as stroke, subarachnoid hemorrhage, and brain trauma, but it is also thought to be the mechanism of the migraine aura. It is therefore expected to occur over a range of conditions including the awake behaving state. Yet it is unclear how such a massive depolarization could occur under relatively benign conditions. Using a microfluidic device with focal stimulation capability in a mouse brain slice model, we varied extracellular potassium concentration as well as the area exposed to increased extracellular potassium to determine the minimum conditions necessary to elicit CSD. Importantly, we focused on potassium levels that are physiologically plausible ( $\leq 145$  mM; the intracellular potassium concentration). We found a strong correlation between the threshold concentration and the slice area exposed to increased extracellular potassium: minimum area of exposure was needed with the highest potassium concentration, while larger areas were needed at lower concentrations. We also found that moderate elevations of extracellular potassium were able to elicit CSD in relatively small estimated tissue volumes that might be activated under noninjury conditions. Our results thus show that CSD may be inducible under the conditions that expected in migraine aura as well as those related to brain trauma.

cortical spreading depression; microfluidics; migraine

CORTICAL SPREADING DEPRESSION (CSD) is a fundamental response to brain injury. A propagating wave of massive gray matter depolarization, CSD has been incontrovertibly shown to occur in human brain insults, including stroke, subarachnoid hemorrhage, and trauma (Lauritzen et al. 2011). CSD is also highly conserved in phylogeny, occurring in all mammals tested, as well as birds, reptiles, fish, and amphibians (Marshall 1959; Young 1980). CSD-like events even occur in insects in situations of systemic stress, where they appear to convey an adaptive advantage (Rodgers et al. 2007; Armstrong et al. 2009).

Yet, there is very strong circumstantial evidence that CSD also occurs in migraine, a condition in which no apparent brain injury or massive systemic stress occurs (Olesen et al. 1981; Woods et al. 1994; Cao et al. 1999; Bowyer et al. 2001; Hadjikhani et al. 2001). Moreover, unlike in stroke, subarach-

noid hemorrhage, or trauma, humans undergoing migraine aura are conscious and able to report their experience (Russell and Olesen 1996). This implies that CSD must be inducible under conditions of relative physiological normalcy.

Previous models of CSD, however, have largely been limited to massive ionic, metabolic, or traumatic insults that would not be compatible with the awake, behaving, and apparently uninjured state of migraine (Somjen 2001; Charles and Brennan 2009). It is important to know whether there are conditions that would allow induction of CSD without overt injury.

A first step in understanding the “naturalistic” induction of CSD is to systematically study conditions that will set off this all-or-none event. The pioneering work of Matsuura and Bureš (1971) estimated that a surprisingly large volume of tissue,  $\sim 1$  mm<sup>3</sup>, might be required to initiate CSD in rat brains in vivo under high-potassium solution stimulation. However, their approach necessarily involved unintended damage to superficial cortical layers and lack of explicit control of stimulation areas. This may have led to significant overestimation of “minimum” tissue volumes required for CSD induction.

We previously reported the development of a microfluidic device that allows precise focal control of chemical environments of a brain slice (Tang et al. 2011). By locally applying solutions of different concentrations of potassium ions over different areas of the cortical layers of mouse brain slices, we study conditions necessary for CSD induction. We find that CSD is inducible under a wide range of physiologically plausible parameters, with smaller stimulation areas necessary during exposure to extracellular potassium levels ( $[K^+]_e$ ) expected in trauma and significantly larger stimulation areas necessary under  $[K^+]_e$  expected without overt injury. Our data thus define a set of conditions upon which the physiologically realistic modeling of CSD (in silico, in vitro, and in vivo) may proceed.

### MATERIALS AND METHODS

**Ethical approval.** Experimental protocols were approved by the Animal Research Committees of University of California, Los Angeles, California and the University of Utah.

**Brain slice preparation and maintenance.** Male C57Bl/6 mice (age: 1–3 mo;  $n = 22$ ) were deeply anaesthetized with isoflurane and decapitated. The brain was rapidly removed and immersed in an ice-cold high-sucrose low-sodium artificial cerebrospinal fluid (ACSF) solution of the following composition (in mM): 216 sucrose, 2 KCl, 2 MgSO<sub>4</sub>, 1.25 NaH<sub>2</sub>PO<sub>4</sub>, 2 CaCl<sub>2</sub>, 1 MgCl<sub>2</sub>, 26 NaHCO<sub>3</sub>, and 10 glucose bubbled with 95% O<sub>2</sub>-5% CO<sub>2</sub>. The brain was then glued to a stage, and coronal slices of 400- $\mu$ m thickness were cut in an ice-cold

\* Y. S. Ju and K. C. Brennan contributed equally to this work.

Address for reprint requests and other correspondence: K. C. Brennan, Dept. of Neurology, Univ. of Utah, 383 Colorow Dr., Rm. 364, Salt Lake City, UT 84108 (e-mail: k.c.brennan@hsc.utah.edu).

oxygenated sucrose solution using a vibratome (MA752 Motorised Advance Vibroslice; Campden Instruments). The slices were then incubated in an oxygenated ACSF solution (in mM: 125 NaCl, 3 KCl, 1.25  $\text{NaH}_2\text{PO}_4$ , 2  $\text{CaCl}_2$ , 1  $\text{MgCl}_2$ , 25  $\text{NaHCO}_3$ , and 10 glucose) at room temperature for at least 1 h before the experiments.

**Microfluidic brain slice chamber.** The microfluidic device and experimental setup is shown in Fig. 1. The device, described in detail in our prior work (Tang et al. 2011), includes embedded microchannels, microposts, and fluidic ports made of polydimethylsiloxane (PDMS). These microstructures are designed to mechanically support a brain slice and focally deliver a specific chemical stream. The outer chamber walls allow a continuous bath perfusion of ACSF to maintain slice viability.

The slice rests on a network of microposts that allow bath perfusion of the underside as well as the top surface of the brain slice. At select locations, the posts are replaced by fluidic port assembly. For each assembly, one application port is surrounded by several suction ports to create a confined chemical plume, which delivers chemicals into a brain slice by diffusion.

Underneath the microposts and ports are microchannels, which connect to an injection pump and a suction pump for fluidic delivery and removal, respectively. Sections of silicone tubing (ID: 1/8") are bonded to the inlets and outlets of the microchannels. A syringe pump (sp100i Pump; WPI, Sarasota, FL) is used to deliver an ACSF solution with a set potassium concentration ( $[\text{K}^+]$ ) into each application port. A vacuum pump (BUCHI V-700, New Castle, DE) with a feedback pressure control module is used to adjust suction flows (mean velocities of the order of 0.01 m/s) and achieve a controlled confined plume of a potassium-rich ACSF solution.

**Plume control and size determination.** Figure 1C shows images of the plume of an ACSF solution labeled with fluorescein over a fluidic port with and without suction, demonstrating that we can successfully confine the plume by a purely fluidic control without requiring any physical seals. The images are shown without a brain slice placed over the fluidic port for clarity, but the creation of a confined plume in the presence of a brain slice was also demonstrated as discussed in previous work (Tang et al. 2011; Fig. 2C).

To determine conditions for CSD induction in terms of the area of a chemically stimulated cortical layer, we used fluidic ports of different radii. The radius of each port was defined as the distance from the port center to the inner boundary of the suction ports (Fig. 2A, *top inset*). The port radii used in the present work were 0.1, 0.15, 0.2, 0.25, 0.36, and 0.5 mm.

Because of the complexity of light diffraction and scattering within a brain tissue, we empirically determined a correlation between the

plume radius under a brain slice and fluorescence images using partially exposed fluidic ports as illustrated in Fig. 2A. The plume radius correlated well with the physical port radius, falling within the range defined by the inner and outer boundaries of the suction ports shown as the dashed lines.

We report normalized plume radius throughout. Plume area was calculated by measuring the area above 50% pixel intensity and using the circle area equation to derive an equivalent or normalized radius to allow comparison. Normalized radius was used because in seven experiments (1 with 0.15-mm port size, 1 with 0.2-mm port size, 1 with 0.25-mm port size, 2 with 0.36-mm port size, and 2 with 0.5-mm port size), port size and positioning were such that the plume boundary was outside the slice boundary. In these cases, the area of the plume over the slice was not circular.

**Induction and optical recording of CSD in brain slices.** Brain slices were transferred from a tissue culture incubator to the microfluidic device maintained at  $32 \pm 1^\circ\text{C}$ , with a continuous ACSF bath perfusion bubbled with 95%  $\text{O}_2$ -5%  $\text{CO}_2$ . This bath solution was delivered to the chamber using gravity at 2 ml/min. A piece of filter paper was placed at the bath outlet to minimize flow fluctuations. The perfusion rate was verified using an analytic balance, and the chamber temperature was monitored and kept within  $32 \pm 1^\circ\text{C}$  throughout the experiment.

CSD was induced by applying a high- $[\text{K}^+]$  oxygenated ACSF solution containing different molarities of KCl substituted for equimolar NaCl. A small amount of fluorescein ( $< 0.1\%$ ) in the ACSF solution allowed visualization of the plume (Fig. 2C). If no CSD was observed for the first set value of the potassium ion concentration, the concentration was increased in steps of 2–10 mM until we reached a threshold concentration. The molarities were 10, 12, 15, 25, 30, 40, 60, 70, 80, 120, 130, and 140 mM above normal ACSF  $[\text{K}^+]$ ; thus total  $[\text{K}^+]$  was 13, 15, 18, 28, 33, 43, 63, 73, 83, 123, 133, and 143 mM. Once a CSD event was observed in these ascending thresholding experiments, we conducted a confirmative experiment by returning to the lower concentration from a prior step and verifying that no CSD would be induced below the detected threshold. To ensure that there was not a systematic bias inherent to our ascending thresholding procedure, we also performed reverse experiments where we began at high values of  $[\text{K}^+]$  applied on the slice surface and then decreased the applied potassium concentration step by step until a minimum threshold level was reached. We observed no difference in the thresholds obtained using the two procedures.

At least three experiments were conducted for each combination of port size and applied potassium ion concentration. To consider a limiting case of an infinitely large application port, additional exper-

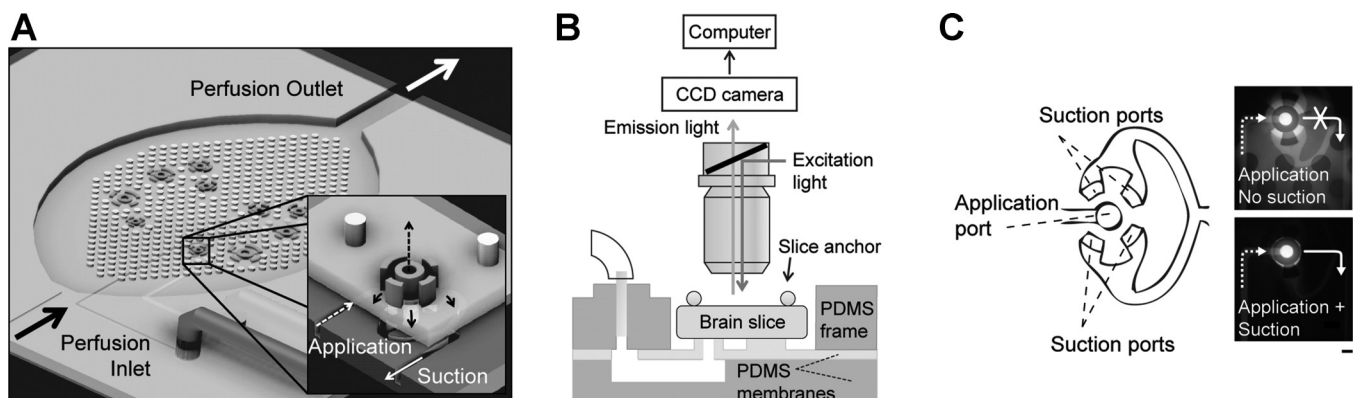


Fig. 1. Microfluidic slice chamber allowing controlled focal depolarization. *A*: brain slice rests on posts in a modified submerged slice chamber. Posts allow bath perfusion both above and below the slice. Selected posts are replaced by microfluidic ports, consisting of 1 application port and 4 suction ports. *Inset* shows 1 microfluidic fluidic port, and dashed arrows represent application flow, solid arrows represent suction flow. Use of the suction ports allows a plume of high- $\text{K}^+$  concentration ( $[\text{K}^+]$ ) solution to be precisely confined. Ports are made of varying sizes, and concentration of perfusion solution is varied. *B*: schematic of the experimental setup showing the chamber integrated with epifluorescence imaging. *C*: schematic view of 1 application/suction port (*left*) and fluorescence images of the applied flows with suction (*right, top*) and without (*right, bottom*). Scale bar = 0.1 mm. PDMS, polydimethylsiloxane.

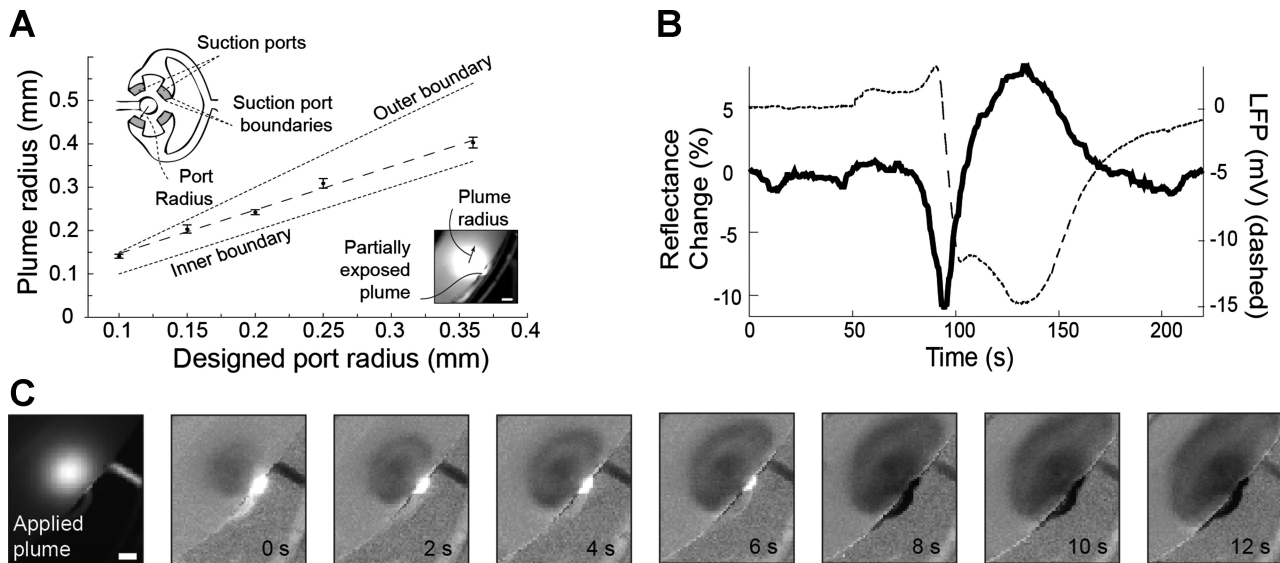


Fig. 2. Optical characterization of cortical spreading depression (CSD) induced by a localized high-[K<sup>+</sup>] plume. **A**: dependence of plume radius on microfluidic port radius. The measured plume sizes reside within the range defined by the inner and outer boundaries of the suction ports. Bars indicate SE. *Bottom inset*: fluorescence image from a partially covered microfluidic port used for plume size determination (see text). Scale bar = 0.1  $\mu$ m. **B**: simultaneous recording of the extracellular DC potential (dashed line) and reflectance change (solid line) during cortical spreading depression. Optical signals were measured concentric with the recording electrode. LFP, local field potential. **C**: reflectance optical intrinsic signal changes during a CSD wave triggered by a localized application of a high-[K<sup>+</sup>] artificial cerebrospinal fluid (ACSF) solution. Images show the fluorescent plume used for stimulation (1st image from left) followed by typical optical changes recorded during the propagating CSD wave. The bright and dark signal outside the slice boundary (bright at 0–6 s, dark 4–12 s) represents passage of fluorescein-labeled K<sup>+</sup> through microfluidic ports. Scale bar = 0.2 mm.

iments were conducted where a potassium-rich ACSF solution was applied over an entire slice via bath perfusion rather than through a microfluidic port.

During each experiment, the applied potassium concentration was maintained at a set value for 2 min or until CSD was observed, whichever was shorter. The fluidic port was then flushed with a solution of oxygenated ACSF at a normal potassium ion concentration, and the slice was allowed to rest for 10 min before retesting. At the end of each experiment, the viability of the slice was confirmed by a successful CSD induction with suprathreshold stimulation areas (elicited by stopping suction at the suction ports, allowing a larger plume to form; or with higher [K<sup>+</sup>]). If the confirmative CSD could not be induced with suprathreshold stimulations, results of that slice were excluded from analysis.

The brain slice was imaged using a  $\times 4$  objective (UPlanSApo; Olympus America, Melville, NY) coupled to a high sensitivity camera (Mightex CCE-B013-U, Pleasanton, CA). Blue light-emitting diode (LED) light (470 nm, half width 25 nm; Luxeon III; Phillips Lumileds) was passed through a filter cube (excitation  $470 \pm 20$  nm, dichroic 505 nm, emission  $>515$  nm; Chroma Technology) for epifluorescence imaging (Fig. 1B). A green LED (500–540 nm) directly illuminated the slice for optical intrinsic signal imaging (Fig. 2C). Images were acquired at 2 Hz; pixel size was 2.2  $\mu$ m.

Epifluorescence and reflected light imaging were alternated to allow detection of the fluorescent plume as well as the intrinsic signal changes caused by CSD. One frame of epifluorescence was collected for every 60 frames of intrinsic signal until CSD was detected, at which point imaging continued with intrinsic signal until the CSD wave had propagated across the imaged region.

*Calculation of the affected cortical volume using simulations.* We used numerical modeling (Tang et al. 2011) to help estimate the potassium-ion-affected tissue volume under each experimental condition. Briefly, the Navier-Stokes equations were solved to calculate the velocity field around each fluidic port. The time-dependent convection-diffusion equation for mass transport was then coupled to the Navier-Stokes equations to predict the concentration profile inside the slice as a function of time. Local injection and suction rates were

adjusted so that the resulting slice bottom plume area matched with those measured in thresholding experiments. Cellular uptake or other active transport mechanisms were not considered.

*Indirect confirmation of the mass transport model using two-photon microscopy.* We performed two-photon microscopy experiments to determine the concentration profile of fluorescein isothiocyanate-dextran molecules (FITC-dextran, 3,000–5,000 molecular weight; Sigma; dissolved in ACSF) applied to a brain slice using one microfluidic port size (0.25- $\mu$ m radius) and compared the experimental results with our model prediction.

Experiments were performed using a Sutter movable objective microscope coupled to a Ti:sapphire laser (MaiTai HP, Spectra Physics, CA) tuned to 810 nm for FITC-dextran and sulforhodamine 101 excitation. A high numerical aperture water-immersion objective (Carl Zeiss W Plan-Apochromat  $\times 20/1.0$  DIC) was used. When necessary, two channels were simultaneously acquired using Chroma filters [535/50 nm (green) and 610/75 nm (red)]. Scanimage (Pologruto et al. 2003) was used to control image acquisition.

Three-hundred-micrometer-thick brain slices were incubated in an ACSF solution with 1  $\mu$ M sulforhodamine 101 (SR101; Invitrogen, Carlsbad, CA) added at 32°C for at least 30 min. SR101 labels astrocytes throughout the thickness of a slice (Nimmerjahn et al. 2004) and thereby allows anatomical registration of two-photon images. Before each optical scan, the location of the slice top surface was first determined by lowering the microscope focus until the first image of where SR101 stained astrocytes (red) became visible. Images were acquired with a  $z$ -axis step size of 10  $\mu$ m from the first image where astrocytes were identified down to the bottom of the slice.

Fluorescence intensity decays with depth  $z$  due to light scattering and absorption by the slice (Helmchen and Denk 2005), which can be modeled using the Beer-Lambert law:

$$F_{2\text{PLSM}} \propto P_0^2 \times e^{-2z/l_s} \quad (1)$$

Here  $F$  is the fluorescent intensity,  $P_0$  is the laser power applied,  $z$  is the depth, and  $l_s$  is the mean free path describing the scattering properties of the tissue (Helmchen and Denk 2005). The fluorescence

intensities in the acquired images were scaled with Eq. 1 using the values of  $P_0$  and  $z$  recorded in the experiments. The optical mean free path is estimated to be  $\sim 140 \mu\text{m}$  from measured variations in the intensity of fluorescence from SR101-labeled astrocytes. This value is consistent with previously reported values of  $50\text{--}200 \mu\text{m}$  (Taddeucci et al. 1996; Oheim et al. 2001; Yaroslavsky et al. 2002).

## RESULTS

**Reliability of CSD induction and recording.** CSD waves were successfully induced by locally applying a solution of potassium rich ACSF onto cortical layers of mice brain slices. CSD was observed as an approximately concentric propagating wave of decreased, followed by increased, light reflectance (Fig. 2C), propagating out from the port site at a speed of  $\sim 3 \text{ mm/min}$  (median: 3.0, 25, 75 percentile 2.3, 3.7 mm/min).

Approximately three to four CSD waves could be induced in a given slice at each test location over periods  $>1 \text{ h}$ . In preliminary experiments we also used direct current field potential recordings (Fig. 2B) to verify that the optical signature of brain slice CSD was indeed accompanied by its electrophysiological correlates (ACSF-filled  $2 \text{ M}\Omega$  resistance glass electrode advanced  $200 \mu\text{m}$  into slice, A-M Systems 700 amplifier, band pass  $0\text{--}1 \text{ kHz}$ , digitized at  $1 \text{ kHz}$ ).

CSD was only induced during superfusion of high- $[\text{K}^+]$  ACSF solutions. We never observed spontaneous CSD induction ( $n = 242$  inductions, 102 experiments), confirming that any effect of unintended mechanical stimulation from the chemical plumes or fluidic ports was negligible. Our microfluidic port design with balanced suction and application flows ensures that the primary delivery mechanism of potassium ions is diffusion rather than the mechanical effects of direct injection.

**Conditions for CSD induction.** Figure 3 shows the potassium concentrations that resulted in CSD induction for different values of the plume radius. The threshold area increased rapidly with decreasing  $\text{K}^+$  concentrations below  $\sim 30 \text{ mM}$ ,

and the threshold concentration increased rapidly with decreasing plume radii below  $\sim 0.4 \text{ mm}$ . The minimum plume radius at which we could induce CSD under physiological concentrations ( $\leq 145 \text{ mM}$ ; or intracellular  $[\text{K}^+]$ ) was  $0.18 \text{ mm}$ . We were unable to elicit CSD at physiological concentrations with smaller plume radii. At subthreshold concentrations, CSD could not be induced even when the chemical stimulation was applied for up to  $2 \text{ min}$ .

Our data show that the concentration of applied potassium ions alone does not govern CSD induction. A fit to the CSD in Fig. 3 suggests a relation of the form:

$$C_{\text{min}} r^2 \sim \text{constant} \quad (2)$$

where  $C_{\text{min}}$  is the minimum applied potassium ion concentration for CSD induction and  $r$  is the corresponding plume radius. Our fitting result shows that the minimum CSD induction condition is a strong correlate of the surface area ( $r^2$ ) of the brain slice that is exposed to high  $[\text{K}^+]$ .

The minimum concentration required to evoke CSD was  $\sim 15 \text{ mM}$ , which was achieved with bath perfusion. An extrapolation of Eq. 2 yields the minimum plume radius corresponding to this concentration of  $\sim 0.57 \text{ mm}$  at this concentration. Bath perfusion experiments at  $13 \text{ mM}$  ( $n = 4$ ) did not achieve CSD induction.

Due to a finite pumping speed, it took (means  $\pm \text{SD}$ )  $17 \pm 8 \text{ s}$  for the plumes to reach  $90\%$  of the final stimulation areas. CSD was induced relatively quickly thereafter, on average after  $12 \text{ s}$  (mean CSD initiation time  $29 \pm 8 \text{ s}$ ). There was no explicit dependence of time-to-CSD-induction on the plume size or potassium ion concentration.

**Minimum tissue volume for CSD induction.** CSD both in vitro and in vivo is a three-dimensional phenomenon; its initiation thus occurs in a volume of tissue, whose parameters constrain the physiological mechanisms of induction. We used our plume area/concentration data and numerical simulation (Tang et al. 2011), validated with two-photon microscopy plume imaging, to estimate the minimum depolarized tissue volumes necessary for CSD initiation (Fig. 4).

To account for the hindered diffusion due to ion movements in tortuous pathways within the brain slice, the diffusivity of  $\text{K}^+$  in free medium ( $2 \times 10^{-9} \text{ m}^2/\text{s}$ ) is reduced to represent the apparent diffusion coefficient (ADC),

$$D_{\text{Apparent}} = \frac{D}{\lambda^2} \quad (3)$$

Here  $\lambda$  is the tortuosity of the brain extracellular space. The value of  $\lambda$  employed in our simulation was either  $1.8$  or  $2.2$ , which are the upper and lower limits of ADC reported in independent previous studies (Nicholson 1993; Nicholson and Tao 1993; Binder et al. 2004; Syková and Nicholson 2008; Zador et al. 2008).

Figure 4A uses these parameters to generate an expected plume profile through a  $400\text{-}\mu\text{m}$  brain slice over time:  $y$  axis is the distance from slice bottom;  $x$  axis is the shows extracellular  $[\text{K}^+]$ , relative to the slice surface. Traces are at  $10\text{-s}$  intervals. There is a clear time dependence to plume concentrations that needs to be incorporated for precise plume modeling. Note that the depth of the affected cortical volume is determined primarily by the diffusion of potassium ions into a brain slice, which is in turn a function of the time. Since the onset of CSD

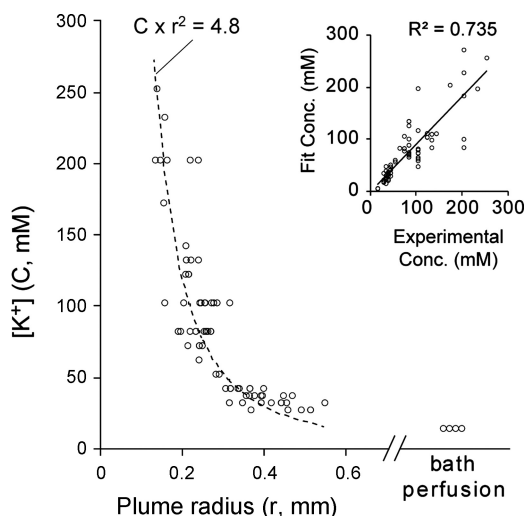


Fig. 3. Minimum conditions for CSD induction. The minimum extracellular  $[\text{K}^+]$  ( $[\text{K}^+]_e$ ) at which CSD could be induced was  $15 \text{ mM}$ , using bath perfusion. At physiologically plausible  $[\text{K}^+]$ ,  $<145 \text{ mM}$ , the minimum plume radius was  $0.18 \text{ mm}$ . Between these limit values, CSD triggering occurred along a line with an approximately constant relation between concentration and square of radius (inset shows data fit);  $n = 69$  CSD inductions, 50 slices, 22 mice.

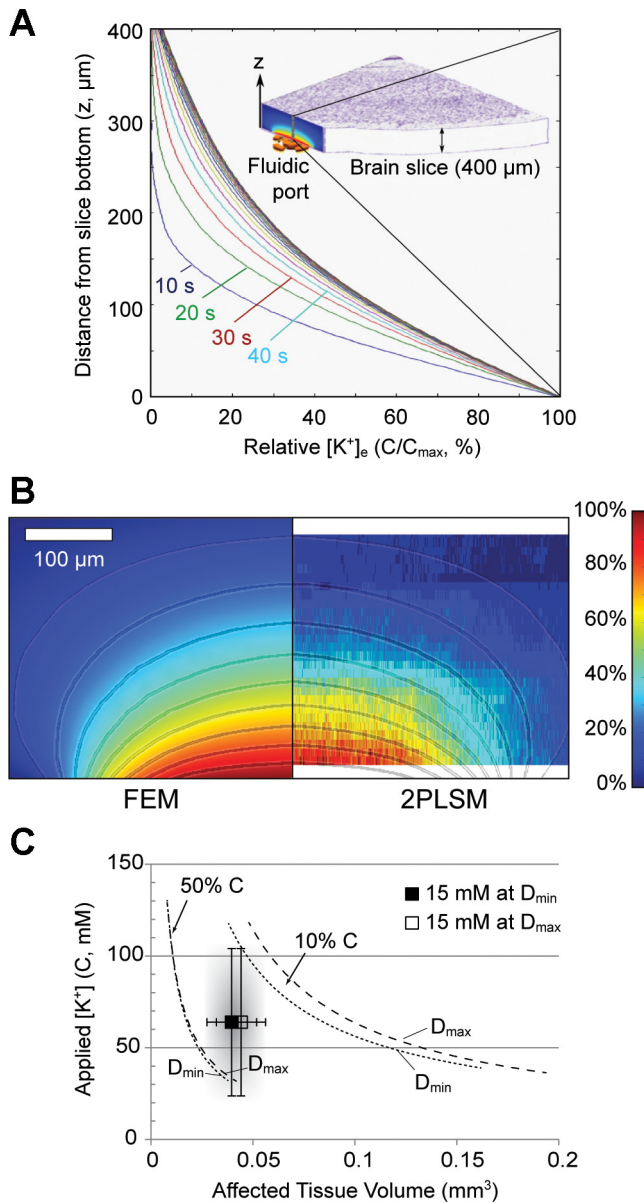


Fig. 4. Minimum cortical volumes required for CSD induction. **A**: time-dependent  $\text{K}^+$  plume modeling. Predicted extracellular potassium concentration is plotted across the slice thickness at the port center location as a function of time. The concentration at each location increases as a function of time due to continuous supply of high- $[\text{K}^+]_e$  solution at the slice bottom surface. A schematic of the slice model is shown in the *inset*. Concentration is plotted along the dotted line above the port center. **B**: validation of model with two-photon microscopy. *Left*: predicted concentration profiles superimposed with isoconcentration contours from 10 to 90% of the applied solution concentration. *Right*: experimentally determined fluorescent intensities across the thickness of a slice. The experimental profile is truncated by the presence of dead cell layers on both surfaces of the slice that did not result in fluorescence signals from SR101 staining. FEM, finite element method; 2PLSM, 2-photon laser scanning microscopy. Scale bar = 0.1 mm. **C**: minimum tissue volumes for CSD induction. Contour lines show expected volumes of  $\text{K}^+$  plume at 50 and 10% of the slice surface concentration. Contours are plotted for minimum ( $D_{\text{min}}$ , dots) and maximum ( $D_{\text{max}}$ , dashes) diffusion constants reported in the literature. Expectation is that CSD volumes would fall within these contours; closer to 50% line. Experimentally determined plume radii at different applied  $[\text{K}^+]_e$  were used to predict the volume of tissue exposed to  $[\text{K}^+]_e > 15$  mM (the minimum concentration for induction). Symbols show mean and standard deviation tissue volumes and applied  $[\text{K}^+]_e$  for minimum ( $D_{\text{min}}$ , black) and maximum ( $D_{\text{max}}$ , white) diffusion constants. Predicted minimum tissue volumes for CSD induction range from 0.03 to 0.06  $\text{mm}^3$ .

occurred relatively shortly ( $< 30$  s) after the application of a potassium-rich ACSF solution, the diffusion depths were relatively small and the depth-to-diameter ratio of the affected cortical volume was predicted to be  $< 0.3$  (approximating a bulged disk).

To further assess the accuracy of the model, we performed two-photon laser scanning microscopy experiments to determine the concentration profile of a plume labeled with FITC-dextran (3,000–5,000 molecular weight; Sigma; dissolved in ACSF) applied to a brain slice using one microfluidic port size (0.25-mm radius) and compared the experimental results with our model prediction. FITC-dextran rather than fluorescein was used to confine the fluorescent plume to the extracellular space. Figure 4B shows the two-dimensional concentration profiles across a slice thickness obtained using the numerical simulation or two-photon microscopy experiments. The two profiles agree reasonably well with each other, validating, albeit indirectly, our numerical model.

With an approximation of time-dependent plume expansion in the brain slice, we were able to use our experimental results to predict the expected volume of tissue necessary to trigger CSD. Figure 4C shows the expected tissue volume necessary to trigger CSD at different concentrations of applied  $\text{K}^+$ . Dashed and dotted curves enclose the expected volumes of tissue exposed to 50 and 10% of the applied  $[\text{K}^+]_e$ : these give a range of expected plume volumes in the tissue. Depending on the concentration, CSD would be more or less plausible within these bounds, for example, based on our experimental data CSD would be very unlikely at the 10% concentration curve, except with the highest concentrations of applied  $\text{K}^+$ . Because the plume volume depends on tissue diffusion coefficient, we plot expected plume volumes at the minimum and maximum diffusivities ( $D_{\text{min}}$ , dots;  $D_{\text{max}}$ , dashes) reported in the literature. Next, we use our experimental data to plot the volume of depolarized tissue expected to induce CSD. We used experimentally determined plume area at each experimentally applied  $[\text{K}^+]_e$  to predict the volume of tissue  $> 15$  mM  $\text{K}^+$ . Our reasoning for using a 15-mM cutoff is that this was the minimum concentration able to induce CSD; we would not expect the volumes enclosed by lower concentrations to be relevant for induction. For each diffusion coefficient ( $D_{\text{min}}$ , black;  $D_{\text{max}}$ , white), the mean and standard deviation tissue volumes and applied  $[\text{K}^+]_e$ , for volumes of tissue predicted to be  $> 15$  mM, are plotted. The area bounded by the error bars (shaded) represents the expected range of CSD ignition volumes from our experiments. The range of predicted volume of tissue necessary to induce CSD at 15 mM is 0.03–0.06  $\text{mm}^3$ . At a cutoff of 30 mM (the lowest value achieved by a circular focal plume rather than bath perfusion), the range of predicted volume is 0.005–0.012  $\text{mm}^3$ .

## DISCUSSION

CSD is suggested as the physiological mechanism behind the migraine aura. However, it is surprising that such a massive ionic and metabolic event, incontrovertibly seen in conditions of brain injury, could be generated in the awake uninjured brain. CSD does not possess a single threshold; like other phenomena [e.g., the action potential (FitzHugh 1955)] the threshold for all-or-none activity is a multidimensional surface (manifold) (Dahlem and Isele 2013). Our goal was

to sample this surface as completely as possible in a brain slice preparation.

We designed our experiments to address the feasibility of CSD under physiologically realistic conditions. In contrast to most CSD models (Aitken et al. 1998; Ayata et al. 2006; Brennan et al. 2007) we focused on  $[K^+]_e$  that could be expected in vivo, in a range whose maximum was approximate intracellular  $[K^+]$ . This maximum concentration is relevant to situations such as brain trauma or stroke, where cellular lysis occurs. The lower limits of the range were designed to test the “ $K^+$  ceiling,” levels of extracellular  $K^+$  ranging from 10 to  $\sim 20$  mM, beyond which both neuronal and vascular behavior changes dramatically (Somjen et al. 1976; Heinemann and Lux 1977; Somjen 1979; Knot et al. 1996). These concentrations are achievable in vivo during pathological states, such as seizure (Heinemann et al. 1977; Heinemann 1986), that are recoverable without apparent cellular injury. Intermediate levels (30–80 mM) are seen during passage of the CSD wave (Somjen 2001) and are also likely relevant to tissue in the vicinity of brain injury such as a contused or infarcted region.

Matsuura and Bureš (1971) estimated the minimum radius of depolarized tissue necessary for CSD induction to be approximately 600–960  $\mu\text{m}$  and the minimum  $[K^+]_e$  between 12 and 45 mM. No direct correlation between the two quantities was reported.

The range of minimum concentrations reported in the previous study is consistent with our results. However, a minimum affected tissue volume calculated from the minimum radii reported by Matsuura and Bureš is 0.9–3.7  $\text{mm}^3$ . This is much larger than our estimated values of  $\sim 0.03$ – $0.06$   $\text{mm}^3$ .

Such discrepancy may in part be due to differences in preparation (rat vs. mouse brain, in vivo vs. in vitro). Perhaps more importantly, the insertion of a 200- $\mu\text{m}$  diameter capillary in the previous study was likely to have caused damage to superficial cortical layers, which are believed to be most sensitive to depolarization and therefore CSD induction (Marshall et al. 1950; Leão 1951; Világi et al. 2001).

In contrast to these in vivo methods, an advantage of our preparation is that we were able to directly control both the concentration of the potassium ions applied to a cortical surface and the focal area exposed to the depolarizing stimuli. We were also able to directly observe the induction of CSD and precisely measure the surface area of tissue exposed to the depolarizing stimulus. By directly observing and modeling fluid transport in slices, we were also able to predict the minimum volume depolarized with greater confidence.

Our results show that CSD can be induced in small volumes of tissue exposed to high physiological-range  $[K^+]_e$ , as well as larger volumes exposed to lower concentrations. Our combined data show that the relationship between  $[K^+]_e$  and plume area is approximately constant. This implies that susceptibility to CSD might be determined by the total mass of  $K^+$  in the extracellular space. The question then arises whether there is a true equivalence between relatively high- $[K^+]_e$ /small-radius experiments and low- $[K^+]_e$  large-radius experiments: i.e., whether high- $[K^+]_e$ /small-radius stimuli elicit CSD because they are actually generating low- $[K^+]_e$  large-radius area of stimulation due to diffusion. Our data suggest this is not the case because high- $[K^+]_e$ /small-radius experiments did not differ in time to CSD induction from low- $[K^+]_e$  large-radius

experiments. If a diffusion-generated large low concentration plume were being generated, high- $[K^+]_e$ /small-radius experiments would have longer induction times.

At  $[K^+]_e$  below  $\sim 30$  mM, the relationship between  $[K^+]_e$  and plume radius flattened. For any  $[K^+]_e$  in this range, a larger area of exposed cortex was required to generate CSD. This change in behavior may reflect a  $[K^+]_e$  buffering capacity that is operant below, and exceeded above  $\sim 30$  mM. It could also reflect the fact that beyond 0.18-mm port radius, our circular port assemblies overlapped the boundaries of the slice, potentially increasing variability. Finally at  $[K^+]_e < 15$  mM, CSD was not elicitable at any area of stimulation including whole slice superfusion. At 15 mM the relationship between  $[K^+]_e$  and area became completely flat, revealing an absolute minimum threshold for CSD induction. Presumably below this  $[K^+]_e$  buffering mechanisms can counter any increases, at least for the duration of  $[K^+]_e$  elevation in our experimental paradigms.

To summarize, our data suggest a  $[K^+]_e$  buffering capacity that at concentrations  $< 15$  mM is intact, that at concentrations  $< 30$  mM is challenged but still operant, and that at concentrations  $> 30$  mM is essentially saturated. It is likely that different buffering mechanisms are at play.

For computational simplicity and limitation in real-time concentration measurement capabilities, our model considered diffusion as the only mechanism for  $K^+$  ion distribution in the extracellular space. Other physiological  $K^+$  regulation mechanisms need to be considered to fully predict the minimum condition for CSD induction: 1)  $K^+$  release from neuronal and glial activity; 2) active  $K^+$  uptake by neurons and glial cells; 3)  $K^+$  spatial buffer by glial cells; and 4) passive KCl uptake by glial cells (Kraig and Nicholson 1978; Largo et al. 1996; Holthoff and Witte 2000; Walz 2002; MacAulay and Zeuthen 2012). The relative importance of the mechanisms varies based on specific experiment conditions and different brain regions (Kofuji and Newman 2004). Moreover, the relative importance of different mechanisms likely differs at different  $[K^+]_e$ . When  $[K^+]_e$  is below  $\sim 12$ – $15$  mM, active potassium uptake by neurons and glial cells likely plays a significant role in clearing potassium from the extracellular space (Cordingley and Somjen 1978; Xiong and Stringer 2000). Under higher  $[K^+]_e$ , the active uptake of potassium likely saturates (Baker 1968; Walz and Hertz 1982); findings consistent with our results. Finally, experimental conditions could also have affected our results and simulations: 1) slice thickness; 2) vertical distance between plume origin and slice; 3) spatial location of the center of the  $K^+$  plume (as different cortical layers have different CSD susceptibility; Marshall et al. 1950; Leão 1951; Világi et al. 2001); 4) correspondence of fluorescent marker concentrations to  $[K^+]_e$ ; and 5) microfluidic device design.

The control we achieve over the ionic and fluidic environment was not possible without a brain slice preparation. However, an obvious limitation of this approach is that the vascular changes that accompany and likely influence CSD were not sampled. Vascular activity is important because of its homeostatic role in vivo and because cerebral arterioles constrict rather than dilate at  $[K^+]_e$  that induce CSD (Knot et al. 1996). This means that vascular delivery and clearance of metabolites are compromised at precisely the levels of  $[K^+]_e$  where neurons and glia are entering a critical transition to depolarization. Implications will need to be tested in vivo. One might predict

that minimum volumes of depolarization could actually be lower in the presence of a functional vasculature. On the other hand, vascular clearance of potassium ions could slow the approach of  $[K^+]_e$  to threshold values and thus have opposite effects.

Our use of a mouse model may also not completely mimic conditions expected in humans. Mouse neural and cellular density is greater than that of humans, and the neuron/glia ratio is higher (Tsai et al. 2009). The implication is that mouse tissue might support CSD at smaller depolarized volumes than human tissue. The fact that mice are lissencephalic while humans are gyrencephalic is likely not relevant to our slice experiments but has implications for CSD induction and propagation (Dahlem and Hadjikhani 2009).

If CSD occurs in awake behaving humans, as is proposed for the migraine aura, it must occur under conditions that do not result in either incapacitation or lasting injury. The volume of depolarized tissue determined from our experiments is small enough that transient, focal alterations in perfusion or metabolism might be sufficient to set off CSD. In this context it is interesting to note that our predicted minimum volumes of depolarized tissue are similar to the predicted volume of a cortical column (Mountcastle 1997) or penetrating artery territory (Woolsey et al. 1996). One could speculate that a discrete sensory column exposed to excessive stimulation, or a single penetrating artery undergoing reversible spasm, might be sufficient to cause CSD without causing lasting tissue damage.

**Conclusions.** We have used a microfluidic device in mouse brain slice preparation to evaluate the minimum conditions necessary to induce CSD. We find that CSD is inducible under a range of conditions including those likely to be encountered in brain injury and those likely during awake behaving states such as migraine.

#### ACKNOWLEDGMENTS

We thank Dr. Andrew Charles for use of equipment.

Present address of H. E. López-Valdés: Universidad Nacional Autónoma de México, Av Universidad 3000, Ciudad Universitaria, 04510 Ciudad de México, Distrito Federal, México.

#### GRANTS

This work was supported by the National Institute of Neurological Disorders and Stroke Grants NS-059072 and NS-070084 (to K. C. Brennan) and Department of Defense Grant CDMRP PR 100060 (to K. C. Brennan).

#### DISCLOSURES

No conflicts of interest, financial or otherwise, are declared by the author(s).

#### AUTHOR CONTRIBUTIONS

Author contributions: Y.T.T., Y.S.J., and K.C.B. conception and design of research; Y.T.T., J.M.M., J.J.T., P.M.S., H.E.L.-V., and K.C.B. performed experiments; Y.T.T., J.M.M., J.J.T., P.M.S., H.E.L.-V., and K.C.B. analyzed data; Y.T.T., J.M.M., J.J.T., P.M.S., H.E.L.-V., Y.S.J., and K.C.B. interpreted results of experiments; Y.T.T., J.J.T., and K.C.B. prepared figures; Y.T.T. and K.C.B. drafted manuscript; Y.T.T., J.M.M., J.J.T., P.M.S., H.E.L.-V., Y.S.J., and K.C.B. edited and revised manuscript; Y.T.T. and K.C.B. approved final version of manuscript.

#### REFERENCES

Aitken PG, Tombaugh GC, Turner DA, Somjen GG. Similar propagation of SD and hypoxic SD-like depolarization in rat hippocampus recorded optically and electrically. *J Neurophysiol* 80: 1514–1521, 1998.

- Armstrong GA, Rodgers CI, Money TG, Robertson RM. Suppression of spreading depression-like events in locusts by inhibition of the NO/cGMP/PKG pathway. *J Neurosci* 29: 8225–8235, 2009.
- Ayata C, Jin H, Kudo C, Dalkara T, Moskowitz MA. Suppression of cortical spreading depression in migraine prophylaxis. *Ann Neurol* 59: 652–661, 2006.
- Baker PF. Recent experiments on the properties of the Na efflux from squid axons. *J Gen Physiol* 51: 172–179, 1968.
- Binder DK, Papadopoulos MC, Haggie PM, Verkman AS. In vivo measurement of brain extracellular space diffusion by cortical surface photobleaching. *J Neurosci* 24: 8049–8056, 2004.
- Bowyer SM, Aurora KS, Moran JE, Tepley N, Welch KM. Magnetoencephalographic fields from patients with spontaneous and induced migraine aura. *Ann Neurol* 50: 582–587, 2001.
- Brennan KC, Romero Reyes M, López-Valdés HE, Arnold AP, Charles AC. Reduced threshold for cortical spreading depression in female mice. *Ann Neurol* 61: 603–606, 2007.
- Cao Y, Welch KM, Aurora S, Vikingstad EM. Functional MRI-BOLD of visually triggered headache in patients with migraine. *Arch Neurol* 56: 548–554, 1999.
- Charles AC, Brennan KC. Cortical spreading depression—new insights and persistent questions. *Cephalalgia* 29: 1115–1124, 2009.
- Cordingley GE, Somjen GG. The clearing of excess potassium from extracellular space in spinal cord and cerebral cortex. *Brain Res* 151: 291–306, 1978.
- Dahlem MA, Hadjikhani N. Migraine aura: retracting particle-like waves in weakly susceptible cortex. *PLoS One* 4: e5007, 2009.
- Dahlem MA, Isele TM. Transient localized wave patterns and their application to migraine. *J Math Neurosci* 3: 7, 2013.
- FitzHugh R. Mathematical models of threshold phenomena in the nerve membrane. *Bull Math Biophys* 17: 257–278, 1955.
- Hadjikhani N, Sanchez Del Rio M, Wu O., Schwartz D, Bakker D, Fischl B, Kwong KK, Cutrer FM, Rosen BR, Tootell RB, Sorensen AG, Moskowitz MA. Mechanisms of migraine aura revealed by functional MRI in human visual cortex. *Proc Natl Acad Sci USA* 98: 4687–4692, 2001.
- Heinemann U, Lux HD, Gutnick MJ. Extracellular free calcium and potassium during paroxysmal activity in the cerebral cortex of the cat. *Exp Brain Res* 27: 237–243, 1977.
- Heinemann U, Lux HD. Ceiling of stimulus induced rises in extracellular potassium concentration in the cerebral cortex of cat. *Brain Res* 120: 231–249, 1977.
- Heinemann U. Excitatory amino acids and epilepsy-induced changes in extracellular space size. *Adv Exp Med Biol* 203: 449–460, 1986.
- Helmchen F, Denk W. Deep tissue two-photon microscopy. *Nat Methods* 2: 932–940, 2005.
- Holthoff K, Witte OW. Directed spatial potassium redistribution in rat neocortex. *Glia* 29: 288–292, 2000.
- Knot HJ, Zimmermann PA, Nelson MT. Extracellular K(+)-induced hyperpolarizations and dilatations of rat coronary and cerebral arteries involve inward rectifier K(+) channels. *J Physiol* 492.2: 419–430, 1996.
- Kofuji P, Newman EA. Potassium buffering in the central nervous system. *Neuroscience* 129: 1045–1056, 2004.
- Kraig RP, Nicholson C. Extracellular ionic variations during spreading depression. *Neuroscience* 3: 1045–1059, 1978.
- Largo C, Cuevas P, Somjen GG, Martin del Rio R., Herreras O. The effect of depressing glial function in rat brain in situ on ion synaptic transmission, and neuron survival. *J Neurosci* 16: 12219–12229, 1996.
- Lauritzen M, Dreier JP, Fabricius M, Hartings JA, Graf R, Strong AJ. Clinical relevance of cortical spreading depression in neurological disorders: migraine, malignant stroke, subarachnoid and intracranial hemorrhage, and traumatic brain injury. *J Cereb Blood Flow Metab* 31: 17–35, 2011.
- Leão AA. The slow voltage variation of cortical spreading depression of activity. *Electroencephalogr Clin Neurophysiol* 3: 315–321, 1951.
- MacAulay N, Zeuthen T. Glial K(+) clearance and cell swelling: key roles for cotransporters and pumps. *Neurochem Res* 37: 2299–2309, 2012.
- Marshall WH, Hanna C, Barnard G. The relation of dehydration of the brain to the spreading depression of Leao. *Electroencephalogr Clin Neurophysiol* 2: 177–185, 1950.
- Marshall WH. Spreading cortical depression of Leão. *Physiol Rev* 39: 239, 1959.

- Matsuura T, Bureš J.** The minimum volume of depolarized neural tissue required for triggering cortical spreading depression in rat. *Exp Brain Res* 12: 238–249, 1971.
- Mountcastle VB.** The columnar organization of the neocortex. *Brain* 120: 701–722, 1997.
- Nicholson C, Tao L.** Hindered diffusion of high molecular weight compounds in brain extracellular microenvironment measured with integrative optical imaging. *Biophys J* 65: 2277–2290, 1993.
- Nicholson C.** Ion-selective microelectrodes and diffusion measurements as tools to explore the brain cell microenvironment. *J Neurosci Methods* 48: 199–213, 1993.
- Nimmerjahn A, Kirchhoff F, Kerr JND, Helmchen F.** Sulforhodamine 101 as a specific marker of astroglia in the neocortex in vivo. *Nat Methods* 1: 31–37, 2004.
- Oheim M, Beaurepaire E, Chaigneau E, Mertz J, Charpak S.** Two-photon microscopy in brain tissue: parameters influencing the imaging depth. *J Neurosci Methods* 111: 29–37, 2001.
- Olesen J, Larsen B, Lauritzen M.** Focal hyperemia followed by spreading oligemia and impaired activation of rCBF in classic migraine. *Ann Neurol* 9: 344–352, 1981.
- Pologruto TA, Sabatini BL, Svoboda K.** ScanImage: flexible software for operating laser scanning microscopes. *Biomed Eng Online* 2: 13, 2003.
- Rodgers CI, Armstrong GAB, Shoemaker KL, LaBrie JD, Moyes CD, Robertson RM.** Stress preconditioning of spreading depression in the locust CNS. *PLoS One* 2: e1366, 2007.
- Russell MB, Olesen J.** A nosographic analysis of the migraine aura in a general population. *Brain* 119: 355–361, 1996.
- Somjen GG, Rosenthal M, Cordingley GE, LaManna J, Lothman E.** Potassium, neuroglia, and oxidative metabolism in central gray matter. *Fed Proc* 35: 1266–1271, 1976.
- Somjen GG.** Extracellular potassium in the mammalian central nervous system. *Ann Rev Physiol* 41: 159–177, 1979.
- Somjen GG.** Mechanisms of spreading depression and hypoxic spreading depression-like depolarization. *Physiol Rev* 81: 1065–1096, 2001.
- Syková E, Nicholson C.** Diffusion in brain extracellular space. *Physiol Rev* 88: 1277–1340, 2008.
- Taddeucci A, Martelli F, Barilli M, Ferrari M, Zaccanti G.** Optical properties of brain tissue. *J Biomed Optics* 1: 117–123, 1996.
- Tang YT, Kim J, López-Valdés HE, Brennan KC, Ju YS.** Development and characterization of a microfluidic chamber incorporating fluid ports with active suction for localized chemical stimulation of brain slices. *Lab Chip* 11: 2247–2254, 2011.
- Tsai PS, Kaufhold JP, Blinder P, Friedman B, Drew PJ, Karten HJ, Lyden PD, Kleinfeld D.** Correlations of neuronal and microvascular densities in murine cortex revealed by direct counting and colocalization of nuclei and vessels. *J Neurosci* 29: 14553–14570, 2009.
- Világi I, Klapka N, Luhmann HJ.** Optical recording of spreading depression in rat neocortical slices. *Brain Res* 898: 288–296, 2001.
- Walz W, Hertz L.** Ouabain-sensitive and ouabain-resistant net uptake of potassium into astrocytes and neurons in primary cultures. *J Neurochem* 39: 70–77, 1982.
- Walz W.** Chloride/anion channels in glial cell membranes. *Glia* 40: 1–10, 2002.
- Woods RP, Iacoboni M, Mazziotta JC.** Bilateral spreading cerebral hypoperfusion during spontaneous migraine headache. *N Engl J Med* 331: 1689–1692, 1994.
- Woolsey TA, Rovainen CM, Cox SB, Henegar MH, Liang GE, Liu D, Moskalenko YE, Sui J, Wei L.** Neuronal units linked to microvascular modules in cerebral cortex: response elements for imaging the brain. *Cereb Cortex* 6: 647–660, 1996.
- Xiong Z, Stringer JL.** Sodium pump activity, not glial spatial buffering, clears potassium after epileptiform activity induced in the dentate gyrus. *J Neurophysiol* 83: 1443–1451, 2000.
- Yaroslavsky AN, Schulze PC, Yaroslavsky IV, Schober R, Ulrich F, Schwarzmaier HJ.** Optical properties of selected native and coagulated human brain tissues in vitro in the visible and near infrared spectral range. *Phys Med Biol* 47: 2059–2073, 2002.
- Young W.** Spreading depression in elasmobranch cerebellum. *Brain Res* 199: 113–126, 1980.
- Zador Z, Magzoub M, Jin S, Manley GT, Papadopoulos MC, Verkman AS.** Microfiber optic fluorescence photobleaching reveals size-dependent macromolecule diffusion in extracellular space deep in brain. *FASEB J* 22: 870–879, 2008.